ELSEVIER

Journal of Nuclear Materials 290–293 (2001) 12–18

journal of nuclear materials

www.elsevier.nl/locate/jnucmat

# Review of initial experimental results of the PSI studies in the large helical device

S. Masuzaki [a,*], K. Akaishi [a], H. Funaba [a], M. Goto [a], K. Ida [a], S. Inagaki [a], N. Inoue [a], K. Kawahata [a], A. Komori [a], Y. Kubota [a], T. Morisaki [a], S. Morita [a], Y. Nakamura [a], K. Narihara [a], K. Nishimura [a], N. Noda [a], N. Ohyabu [a], B.J. Peterson [a], A. Sagara [a], R. Sakamoto [a], K. Sato [a], M. Shoji [a], H. Suzuki [a], Y. Takeiri [a], K. Tanaka [a], T. Tokuzawa [a], T. Watanabe [a], K. Tsuzuki [b], T. Hino [c], Y. Matsumoto [c], S. Kado [d], O. Motojima [a], LHD Experimental Group

[a] *National Institute for Fusion Science, Oroshi 322-6, Toki 509-5292, Japan*
[b] *Department of Fusion Plasma Research, Japan Atomic Energy Research Institute, 319-1195, Japan*
[c] *Division of Quantum Energy Engineering, Hokkaido University, 060-8628, Japan*
[d] *High Temperature Plasma Center, University of Tokyo, 2-11-16 Yayoi, Bunkyo-ku, Tokyo 113-8656, Japan*

**Abstract**

The large helical device (LHD) is the largest heliotron type superconducting device. Its operation was started on 31 March 1998. Three experimental campaigns have been completed until the end of 1999. Wall conditioning mainly by cleaning discharges using ECRF or glow discharges worked well even without high temperature baking. The plasma production with ECRH and auxiliary heating with NBI and/or ICRF in the LHD configuration equipped with open helical divertor were well performed. The divertor material was SS316L in the first and second campaigns, and was replaced by the graphite in the third campaign. The influences of the different divertor materials were investigated. Our understanding of the edge and the divertor plasma has progressed. Long-pulse discharges 80 and 68 s heated by NBI (0.5 MW) or ICRF (0.9 MW) have been achieved, respectively. No severe limitation of the duration has appeared. 

*Keywords:* Plasma–material interaction; Divertor; Edge plasma; LHD; Plasma facing components

## 1. Introduction

The large helical device (LHD) is a superconducting heliotron type device with a set of $l = 2/m = 10$ continuous helical coils and three sets of poloidal coils [1–8]. The major and the averaged minor radii are 3.9 and 0.65 m, respectively.

The edge plasma control using the divertor for improved confinement and the steady-state operation of high performance plasmas are two of the basic physics objectives of LHD. One hour discharge with input power of 3 MW is a near-term target to establish the physical and technical basis for future steady-state operation.

LHD started its operation on 31 March 1998, and three experimental campaigns have been completed until the end of 1999. In the first campaign, the plasmas were produced and sustained by ECRH (up to ~0.35 MW), and in the second campaign, plasmas were initiated by ECRH at a magnetic strength of 1.5 T, and heated by NBI (up to ~3.5 MW). In the recent experimental campaign, ICRF (up to ~1.5 MW) power has been added and the total heating power became ~5 MW at a magnetic field strength of 2.75 T. Achieved electron and ion temperatures are 4.4 and 3.5 keV, respectively, and the stored energy is up to ~0.88 MJ. A fusion triple

* Corresponding author. Tel.: +81-572 58 2145; fax: +81-572 58 2618.
*E-mail address:* masuzaki@LHD.nifs.ac.jp (S. Masuzaki).

0022-3115/01/$ - see front matter 
PII: S0022-3115(00)00562-6

product ($n\tau$T) of $2 \times 10^{19}$ keV m$^{-3}$ s was achieved. An averaged $\beta$ of 2.4% was obtained with a magnetic field of 1.3 T. Energy confinement time has reached 0.3 s at a maximum, and is enhanced by 15–60% over the ISS-95 scaling, which was derived from the existing medium-sized helical devices [9,10]. The pedestal that exists around $\rho = 0.9$ is considered to be a key factor for this enhanced confinement [10,11]. This paper reviews the initial experimental results on plasma–surface interactions in these three campaigns.

## 2. Subsystems of LHD

### 2.1. Plasma facing components

The plasma facing components of LHD were designed to withstand the long-pulse discharge with 3 MW input power that is planned in the near future. This is the severest operation for plasma facing components in LHD.

#### 2.1.1. Vacuum vessel and the first wall panels

The LHD vacuum vessel is made of SS316L, and the total area including ports is 780 m$^2$ [4]. Water cooling channels were welded on the surface of the vessel to keep the vessel temperature below 70°C with the superconducting coil energized, 95°C otherwise to limit the thermal heat flow into them. Thus, the limit of baking temperature of the vessel is relatively low, 95°C. A number of small panels made of SS316L with Cu clad layer are bolted on the water channels to form the first wall, which will keep the vacuum vessel temperature below 70°C under 3 MW steady-state plasma operation. Installation of the first wall panels have not been completed yet. At the beginning of the third experimental campaign, inboard-side wall in the vertically elongated cross-section that was nearest to the plasma was covered by the panels.

#### 2.1.2. Divertor plates

In the first and second campaigns, the material facing the divertor plasma was SS316L. After the second campaign, actively cooled divertor plates were installed. Each divertor plate consists of an isotropic graphite (IG-430U,TOYO TANSO) armor tile, copper heat sink, water cooling pipe made of SS316L, and graphite sheet, which are fixed with several bolts [12]. For the design of the divertor plate in LHD, the R and D works have been carried out [13]. The heat flux of 0.75 MW/m$^2$ was assumed to be the severest case during the 1 h operation with input power of 3 MW.

### 2.2. Vacuum pumping and monitor system

A manifold with diameter of 1.2 m and length of 10 m is connected to the vacuum vessel from a horizontal port [4]. It is equipped with two cryogenic pumps with a pumping speed of 70 m$^3$/s for $H_2O$, two turbomolecular pumps with a pumping speed of 5 m$^3$/s for $N_2$, two compound turbomolecular pumps with a pumping speed of 1.8 m$^3$/s for $N_2$. The effective pumping speed at the pumping port in vacuum vessel estimated from the pressure decay curve is 42 m$^3$/s for hydrogen, and 8.4 m$^3$/s for helium, respectively [14]. The base pressure of the vacuum vessel is less than $8 \times 10^{-7}$ Pa.

Total and partial pressures are monitored by pressure gauges and quadrupole mass spectrometer. An ASDEX type fast ion gauge located 3 m away from plasma monitored the total pressure during plasma discharges [14].

### 2.3. Plasma diagnostics

During three experimental campaigns, developments of LHD plasma diagnostic systems have been proceeded. The radial profiles of electron and ion temperature and density were provided by YAG-laser Thomson scattering, charge exchange recombination spectroscopy (CXRS) and FIR interferometer, respectively. Thomson scattering and FIR interferometer cover the edge open field layer. For divertor plasma measurements, 'dome' type Langmuir probe arrays were embedded in the divertor plates.

## 3. LHD plasma operation

In LHD, steady-state magnetic field for plasma confinement is generated by the superconducting helical and poloidal coils. In the third campaign, maximum operating magnetic field strength was 2.9 T at the magnetic axis. The position of magnetic axis ($R_{ax}$) can be shifted, and $R_{ax} = 3.6$–$3.9$ m are used for the plasma experiments.

ECRH (82.6, 84 and 168 GHz, up to 0.9 MW) power focused on the magnetic axis which generates plasma, and auxiliary heating power with negative-ion based NBI (hydrogen beam, up to 4.2 MW) and/or ICRF (up to 1.5 MW) increased the plasma stored energy in the third campaign. The plasma volume depends on the magnetic configuration, and is typically about 30 m$^3$.

Particle fueling was provided by using gas-puffing and hydrogen pellet injection. Hydrogen and helium gases are used depending on the experimental aims. Due to the screening effect in the open field layer surrounding the core plasma [15–17], and the wall pumping [14,18,19], the fueling efficiency of gas-puffing is typically 20%. The fueling pellet injection was performed to extend the operational density regime [20]. The fueling efficiency of the pellet injection is 50–90% depending on the electron temperature.

In the second campaign, the strong wall pumping was observed especially during $H_2$ discharges [14]. In the case of hydrogen, about 50% of the injected particles were missing. On the other hand, in the case of helium, almost no particles were missing. These results indicated the difference of recycling between hydrogen and helium. This trend was continued during the second campaign. However in the third campaign, wall pumping property was changed especially for helium, namely, injected helium particles were also absorbed in the wall. The graphite divertor plates are considered to be the sink of helium. The quantitative analysis is under way, and this change of wall pumping property affects the wall conditioning scenario in the third campaign described later.

## 4. Impurity control

The impurity control methods in LHD are wall conditioning and selection of plasma facing materials. In the first and second campaigns, stainless steel is the main plasma facing material, and in the latest campaign, the graphite divertor plates, as mentioned in the previous section, were installed.

### 4.1. Wall conditioning

Wall conditioning in LHD has been done mainly by cleaning discharges and baking at a mild temperature (95°C). Electron cycrotron resonance discharge cleaning (ECR-DC) using the 2.45 GHz microwave and glow discharge cleaning (G-DC) have been utilized for the conditioning. Titanium gettering was also applied for further reduction of oxygen impurity. With 1 h operation of the gettering system, nearly 30% of vacuum vessel wall surface can be covered with more than three monolayers of the titanium film. The heliotron configuration is free from disruption. Therefore, LHD does not suffer from recontamination of the wall by disruption, which results in smooth improvement of the conditioning with high power main discharges.

In Table 1, plasma facing materials and wall conditioning in each experimental campaign are summarized. In the first campaign, only a few hours of ECR-DC was carried out before the production of the first ECRH (82.6, 84 GHz) heated plasma on 31 March 1998. During the first experimental campaign, combination of the ECRH main discharges, 5 kW ECR-DC with helium gas and the titanium gettering improved the wall condition gradually. The total amount of evacuated surface contaminants was over 100 molecular layers [21]. As a result of this procedure, the plasma with stored energy of 16 kJ was achieved, being considered to be well-performed discharge for the target plasma of NBI heating in the second campaign.

After the first campaign, two graphite armors (3 $m^2$) were installed to protect the vacuum vessel from the NB shine through power, and many diagnostics were also installed. He G-DC was used as the main wall-conditioning method to improve the condition of graphite armor and even in the diagnostics ports. After about two months of opening vessel, 10 days of vacuum vessel baking with mild temperature (95°C) was conducted before the starting of plasma experiments in the second campaign, and about 53 molecular layers of surface adsorbates were evacuated. Owing to this preparation, He G-DC could start without any severe arcings [21]. The discharge voltage of He G-DC was about 210 V and the averaged current density at the wall was 36 mA/$m^2$. In LHD, He G-DC cannot be conducted between shots because of the steady magnetic field, but it was done every night after the plasma experiment. With this procedure, wall condition was sustained and gradually improved. After the second campaign, the long-term samples which were set in vacuum vessel were taken out, and surface analysis was applied. The results indicated that the He G-DC affect the inside of the diagnostic ports as expected [22,23].

In the third experimental campaign, actively cooled graphite divertor tiles were installed, and the total area of graphite surface became about 30 $m^2$. After about six months of opening vessel, 12 days of mild baking and about 56 h He G-DC were applied, and NBI heating

Table 1
Plasma facing materials and wall conditioning during 1998 and 1999

| | Plasma facing materials | Wall conditioning |
|---|---|---|
| First campaign (31 March 1998–14 May 1998) | SS316L Total surface area ~780 $m^2$ | He ECR-DC (5 kW) Titanium getter 95°C baking |
| Second campaign (14 September 1998–14 December 1998) | SS316L Graphite (NBI armor) Graphite area ~3 $m^2$ (~0.4%) | He G-DC (6 kW, 210 V, 36 mA/$m^2$) Titanium getter 95°C baking |
| *Installation of the graphite divertor plates* | | |
| Third campaign (13 July 1999–17 December 1999) | SS316L Graphite (NBI armor and the divertor plates) Graphite area ~30 $m^2$ (~4%) | He G-DC $H_2$ G-DC (8.2 kW, 410 V, 26 mA/$m^2$) Titanium getter 95°C baking |

worked well at the very early stage in the third campaign. However, in the hydrogen gas-puff-fueled discharges, a significant helium contamination was observed. This indicated that helium desorbed probably from divertor plates during the discharge, and due to its large recycling rate, helium became dominant after the termination of hydrogen gas-puffing. To avoid the desorption of helium during hydrogen discharge, $H_2$G-DC was applied before the experiment with hydrogen discharges. In $H_2$ G-DC, the typical discharge voltage was about 410 V, and the averaged current density at the wall was 26 mA/m$^2$. Accumulated helium was removed with the time constant of about 1 h. As a result, the working gas for G-DC was changed depending on the working gas of following main discharge.

### 4.2. Influences of plasma facing materials

The differences of the materials facing divertor plasma, that is SS in the first and the second campaigns, and the graphite in the third campaign appeared in radiation profile and spectroscopic measurements [24].

Fig. 1 shows a typical radiation profile obtained by bolometer fan-arrays in the second and third campaigns, respectively [25]. The reduction of radiation power from the core region is clearly seen. On the other hand, the edge radiation was not reduced. These results suggest the decrease of metal impurities. VUV spectroscopy indicated the apparent reduction of iron line intensities, and supports the idea. Due to the cleaning discharges and the bombardment of charge-exchange atoms, the SS first wall was considered to be sputtered, and deposited on the divertor plates. After the third campaign, the surface analysis of the graphite divertor plates has been started. Initial result of the identification of deposited materials on a divertor plate using energy dispersive X-ray spectroscopy (EDS) showed that the main deposited material is iron. Quantitative analysis of the surface composition is in progress.

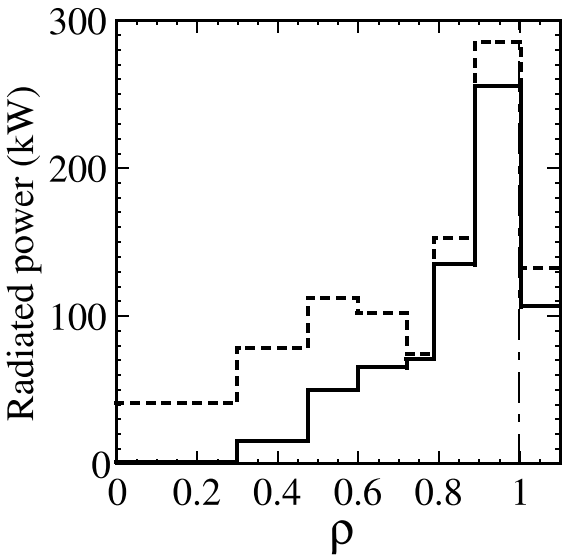


Fig. 1. Radiated power profile on the normalized minor radius. Dashed line: SS divertor plates (#6607, $t = 1.0$ s, $P_{NBI} = 3.0$ MW); solid line: graphite divertor plates (#11562, $t = 1.57$ s, $P_{NBI} = 3.5$ MW).

## 5. Studies of the edge and divertor plasmas

One of the features of the heliotron type magnetic configuration is the structure of open field lines layer surrounding the core region. Stochastic behavior of magnetic field lines is predicted by the calculations of magnetic field tracing, and double-null-like divertor structure is naturally formed [26–29]. The stochastic boundaries have also been studied in tokamaks with ergodic divertor configuration [30,31], and many features are considered to be common to each other. In Fig. 2 [11], typical profiles of the connection length of magnetic field lines, $L_c$, along the major radius at $Z = 0$ in the horizontally elongated poloidal cross-section are shown for different $R_{ax}$.$L_c$ in LHD open field region is much larger than those found at the edge of the large tokamaks in $X$-point configuration.

### 5.1. Profiles of $T_e$ and $n_e$ in the edge open field region

The edge $T_e$ and $n_e$ profiles for different magnetic axis positions ($R_{ax}$) obtained by Thomson scattering are shown in Fig. 2 with the magnetic fields connection length profiles. $T_e$ and $n_e$ profiles appear due to the strong dependence on the magnetic configuration. In the case of $R_{ax} = 3.6$ m, the connection length is short, less than 10 m, between $R = 4.66$ and 4.84 m. Such short field lines connecting to the divertor plates cannot approach the core region. Therefore, $T_e$ and $n_e$ profiles do not extend to the region with short connection length. The profiles are determined by the parallel and perpendicular transports, sources and sinks as in tokamaks. For LHD configuration with stochastic magnetic field lines, the transport mechanisms, which determine edge $T_e$ and $n_e$ profiles are more complicated than $X$-point divertor tokamaks. More detailed $n_e$ and $T_e$ profiles in the open field lines layer are necessary to understand the mechanisms.

### 5.2. Helical divertor properties

#### 5.2.1. Profiles of the divertor particle flux

Helical divertor properties were mainly investigated by using dome type Langmuir probe arrays embedded in divertor plates [17,32] that located different positions.

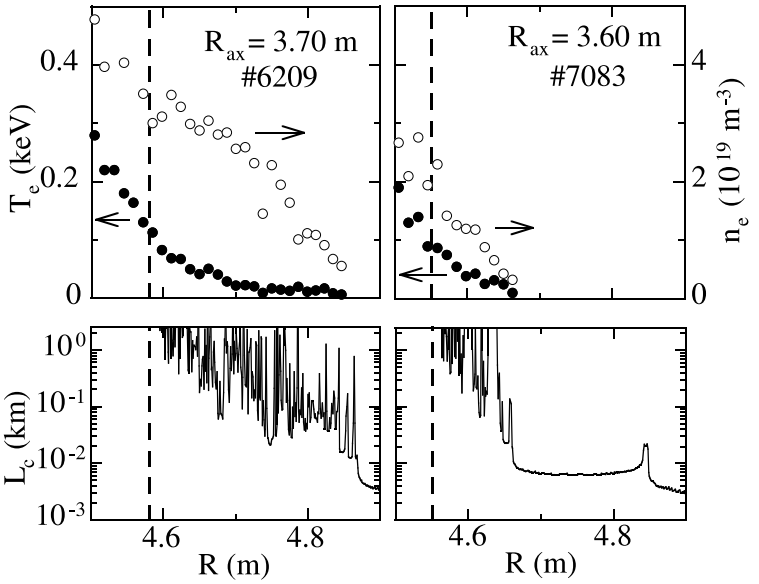


Fig. 2. $T_e, n_e$ and $L_c$ profiles in edge open field region [11]. These profiles are along the major radii in the horizontally elongated cross-section in different magnetic axes. Dashed lines indicate the positions of LCFS.

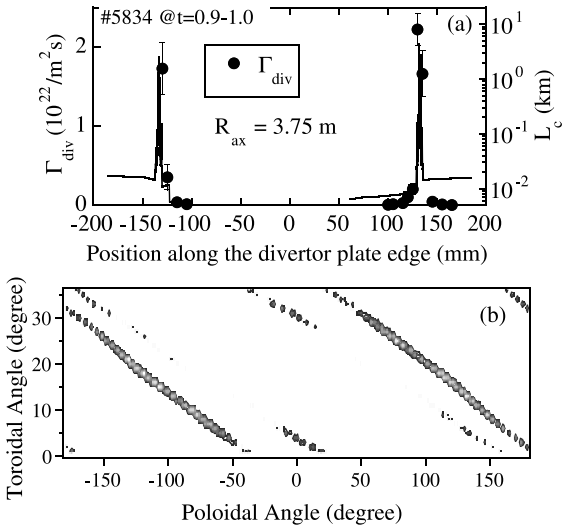


Fig. 3. (a) A typical particles' flux to inboard-side divertor plate and connection length of magnetic field lines. Magnetic axis position ($R_{ax}$) is 3.75 m. (b) Particle deposition profile on the divertor calculated by magnetic field line tracing code with random walk process. ($R_{ax} = 3.75$ m, 1 toroidal section) The poloidal angle of 0 degree indicates the position of torus outboard. The toroidal angle of 0 degree is horizontally elongated cross-section.

The detail configuration of these arrays will be depicted elsewhere [32]. Fig. 3(a) shows the typical particle flux ($\Gamma_{div}$) profile on a divertor plate at the torus inboard-side, and $L_c$ profile calculated along the Langmuir probe array is also indicated. Two peaks of $\Gamma_{div}$ appear at the long $L_c$ positions. As mentioned in the previous section, only long magnetic field lines can approach the core region, thus, the positions of the group of long magnetic field lines become the divertor channels. In the case of other magnetic configuration ($R_{ax}$), similar results were obtained [17]. The widths of the $\Gamma_{div}$ profiles are determined mainly by the $L_c$ profiles, and are insensitive to the local divertor plasma. The decay lengths of the profiles of $\Gamma_{div}$ are generally a few millimeters. For the short $L_c$ beside the long $L_c$ group, the profile does not extend largely. Fig. 3(b) is the particle deposition profile on the divertor for $R_{ax} = 3.6$ m that was calculated by the magnetic tracing with random walk process [29]. Non-uniformity of the deposition profile appears even in the helical direction. Though the particle source is assumed to locate only just inside the last closed flux surface (LCFS) in this calculation, the experimental results of $\Gamma_{div}$ measurements at different divertor plates qualitatively agree with these numerical results.

### *5.2.2. The relationships between the core, edge and divertor plasma*

Electron density and temperature in front of the divertor plates were measured by the single probe characteristics. Fig. 4 shows the line averaged density dependence of divertor plasma density ($n_{e,div}$) and temperature ($T_{e,div}$) in helium discharges ($R_{ax} = 3.6$ m). The line averaged density reached $8 \times 10^{19}$ m$^{-3}$ by gas-puffing. In this regime, $n_{e,div}$ linearly increased with the line

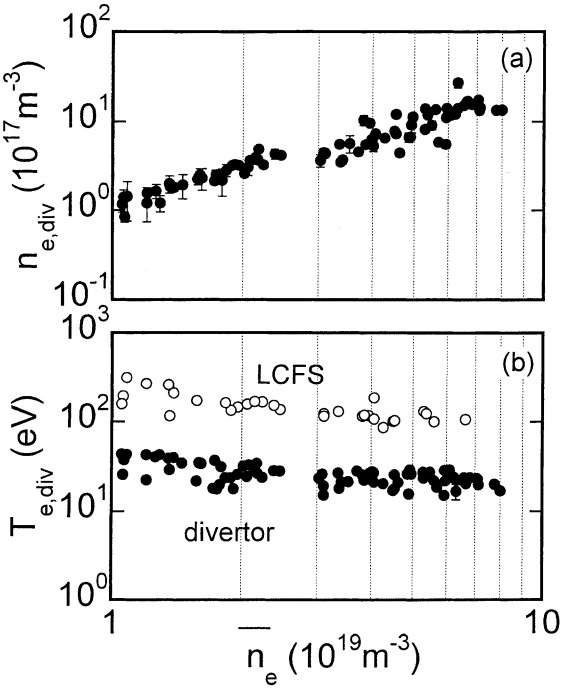


Fig. 4. $n_e$ dependence of $n_{e,div}$, $T_{e,div}$ and $T_e$, LCFS. Helium-puffed discharges, $R_{ax} = 3.6$ m.

averaged density. Electron temperatures at the LCFS are also shown in Fig. 4. Strong reductions of temperature between the LCFS and the divertor plasma are indicated. Electron density is also considered to be reduced largely from Fig. 2. This indicates that the electron pressure is not conserved in the open field layer due to the collisions and viscosity in the long $L_c$. Similar dependence is seen in hydrogen discharges.

## 6. Long-pulse discharge experiment

The long pulse discharge experiment is one of the main experimental programs in LHD. Heating devices, ECRH, ICRF and NBI, have been developed toward the long pulse discharges with high performance plasmas. The first step of experimental target is 1 h operation of the plasma with 3 MW of input power [1–3].

Near the end of the third campaign, the long pulse operation regime was largely extended. Stable discharges were achieved up to 80 s with NBI (0.5 MW) and 68 s with ICRF (0.9 MW) were achieved [33,34]. Fig. 5 shows the time evolutions of plasma parameters during the longest discharge sustained by NBI heating. A high temperature of $T_i = 1.5$ keV at the line averaged density of $1.5–2.0 \times 10^{19}$ m$^{-3}$ was sustained with a low level of radiation power. No significant impurities accumulation

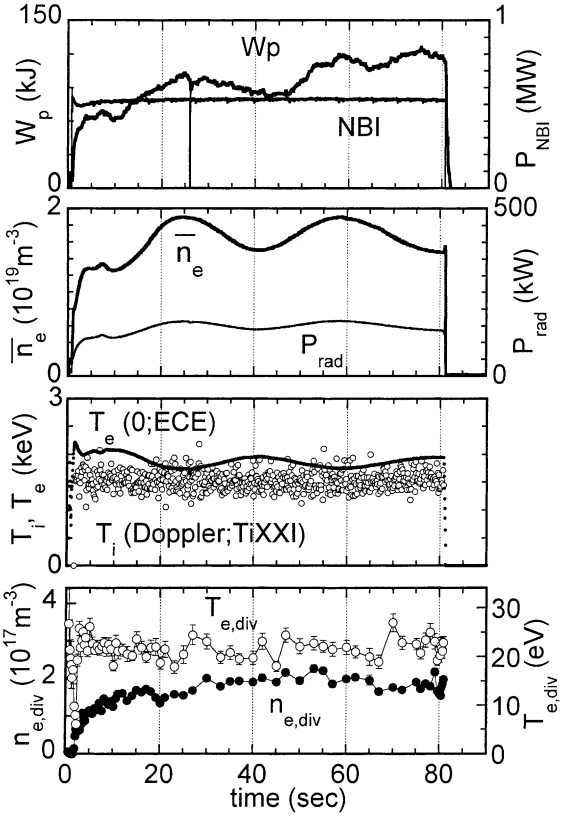


Fig. 5. The time evolutions of the plasma parameters during the longest NBI shot. $P_{NBI} \sim 0.5$ MW, duration time was 80 s.

in the core plasma was observed. The density was well controlled by gas-puffing throughout the discharge. It means that the wall pumping worked until the end of the discharge.

The temperatures of plasma facing components kept rising during the discharge, and did not saturate. The surface temperature of the divertor plates at the torus inboard-side rose up to 80°C. The typical vacuum vessel temperature rose to less than 10°C [33]. The out-gas from such high temperature components was not significant, and as mentioned above, density controllability remains until the end of the discharge. In the divertor, $n_{e,div}$ and $T_{e,div}$ were almost stable, and this is consistent with the small or no out-gas from the divertor. A low-frequency oscillation, the so-called 'breathing', which limited the density rising in the second campaign [35], was not observed in the third campaign. It is considered to be due to the reduction of metal impurity caused by the graphite divertor plates.

At this stage, the pulse length is rather limited by heating systems, for example, the power supply for NBI than plasma wall interactions. The physical limitations such as large amount of out-gas, impurity contamination and deterioration of density controllability have not

appeared with this power level after enough wall conditioning.

## 7. Summary

Initial experimental results related to the PSI studies in LHD have been reviewed. Wall conditioning without high temperature baking has been conducted mainly using glow discharge cleaning, and baking with mild temperature (95°C). After the installation of the graphite divertor plates instead of SS plates, the radiation power from the core plasma was significantly reduced due to the reduction of metal impurity.

Understanding of the edge plasma properties has been in progress. For the stochastic behavior of the magnetic field lines, the mechanisms which determine the $n_e$ and $T_e$ profiles are more complicated than in $X$-point divertor tokamaks. The divertor plasma was investigated by using Langmuir probe arrays embedded in the divertor plates. The particle flux profile on the divertor, such as the peak position and the width are determined mainly by the profile of the connection length of the magnetic field lines. Non-uniform particle deposition profile on the divertor was predicted by the calculation of magnetic field line tracing, and the experimental observation qualitatively agrees with it. Electron density and temperature just in front of the divertor plates largely reduced compared with them at LCFS. This means that pressure is not conserved in the open field lines layer.

The long-pulse discharge experiment has progressed. The durations of 80 s with NBI (0.6 MW) and 68 s with ICRF (0.9 MW) were achieved. The severe limitations of the discharge duration have not appeared in this operational regime. A limitation for the density rising, 'breathing', was not observed in the third campaign. It was caused by the reduction of metal impurity.

## Acknowledgements

The authors gratefully acknowledge Professor M. Fujiwara, Director-General, for his continuous encouragement and support. They would like to thank especially Professor A. Iiyoshi, the former Director-General. The author (S.M.) thanks Dr T. Nagasaka for his technical support for the surface analysis, and Mr N. Suzuki for providing the data of mass-spectrometer.

## References

[1] A. Iiyoshi, et al., Fus. Technol. 17 (1990) 169.
[2] O. Motojima, et al., Plasma Physics and Controlled Nuclear Fusion Research 1990, in: Proceedings of the 13th International Conference 1990, vol. 3. IAEA, Vienna, Washington, DC, 1991, p. 513.
[3] M. Fujiwara, et al., Plasma Phys. Control. Fus. 39 (1997) A261.
[4] A. Iiyoshi, et al., Nucl. Fus. 39 (9Y) (1999) 1245.
[5] O. Motojima, et al., Nucl. Fus. 39 (9Y) (1999).
[6] M. Fujiwara, et al., Plasma Phys. Control. Fus. 41 (1999) B157.
[7] M. Fujiwara, et al., Nucl. Fus. 39 (9Y) (1999) 1659.
[8] O. Motojima, et al., Phys. Plasma 6 (1999) 1843.
[9] U. Stroth, et al., Nucl. Fus. 36 (1996) 1063.
[10] H. Yamada, et al., Phys. Rev. Lett. 84 (2000) 1216.
[11] N. Ohyabu, et al., Phys. Rev. Lett. 84 (2000) 103.
[12] N. Noda, J. Plasma Fus. Res. (1) 1998.
[13] Y. Kubota, et al., Fus. Eng. Des. 39&40 (1998) 247.
[14] H. Suzuki, et al., J. Plasma Fusion Res. (3) (2000) to be published.
[15] S. Morita, et al., in: Proceedings of the 26th EPS conference on Plasma Physics and Controlled Nuclear Fusion, Maastricht, 1999, p. 1321.
[16] S. Motita, et al., in: Proceedings of the 12th Stellarator Workshop, Madison, 1999.
[17] S. Masuzaki, et al., in: Proceedings of the 26th EPS conference on Plasma Physics and Controlled Nuclear Fusion, Maastricht, 1999, p. 1345.
[18] Y. Nakamura, et al., these Proceedings.
[19] Y. Hirooka, et al., these Proceedings.
[20] R. Sakamoto, et al., J. Plasma Fus. Res. (3) (2000) to be published.
[21] A. Sagara, et al., J. Plasma Fus. Res. 75 (1999) 263.
[22] T. Hino, et al., these Proceedings.
[23] N. Inoue, et al., J. Plasma Fus. Res. (3) (2000) to be published.
[24] N. Noda, et al., J. Plasma Fus. Res. (3) (2000) to be published.
[25] B.J. Peterson, et al., these Proceedings.
[26] T. Obiki, et al., Plasma Physics and Controlled Nuclear Fusion Research 1988, in: Proceedings of the 12th International Conference Nice, 1988, vol. 2. IAEA, Vienna, 1989, p. 337.
[27] A. Akao, J. Phys. Soc. Jpn. 59 (1990) 1633.
[28] N. Ohyabu, et al., Nucl. Fus. 34 (1994) 387.
[29] T. Morisaki, et al., Control. Plasma Phys. 40 (2000) 266.
[30] Ph. Ghendrih, et al., Plasma Phys. Control. Fus. 38 (1996) 1653.
[31] Ph. Ghendrih, et al, these Proceedings.
[32] S. Masuzaki, et al., under preparation.
[33] Y. Takeiri, et al., J. Plasma Fus. Res. (3) (2000) to be published.
[34] R. Kumazawa, et al., J. Plasma Fus. Res. (3) (2000) to be published.
[35] B.J. Peterson, et al., Nucl. Fus., to be submitted.